



Remote sensing of phytoplankton functional types in the coastal ocean from the HypsIRI Preparatory Flight Campaign



Sherry L. Palacios^{a,*}, Raphael M. Kudela^b, Liane S. Guild^c, Kendra H. Negrey^b,
Juan Torres-Perez^d, Jennifer Broughton^b

^a Oak Ridge Affiliated Universities, NASA Ames Research Center, Moffett Field, CA, USA

^b University of California, Santa Cruz, Santa Cruz, CA, USA

^c NASA Ames Research Center, Moffett Field, CA, USA

^d Bay Area Environmental Research Institute, NASA Ames Research Center, Moffett Field, CA, USA

ARTICLE INFO

Article history:

Received 16 June 2014

Received in revised form 15 May 2015

Accepted 19 May 2015

Available online 28 May 2015

Keywords:

HypsIRI

Biodiversity

Phytoplankton functional type

Harmful algal bloom

Water quality

Atmospheric correction

PHYDOTax

ABSTRACT

The 2013–2015 Hyperspectral Infrared Imager (HypsIRI) Preparatory Flight Campaign, using the Airborne Visible/Infrared Imaging Spectrometer (AVIRIS) and MODIS/ASTER Airborne Simulator (MASTER), seeks to demonstrate appropriate sensor signal, spatial and spectral resolution, and orbital pass geometry for a global mission to reveal ecological and climatic gradients expressed in the selected California, USA study area. One of the awarded projects focused on the flight transects covering the coastal ocean to demonstrate that the AVIRIS data can be used to infer phytoplankton functional types at the land–sea interface. Specifically, this project directly assesses whether HypsIRI can provide adequate signal in the complex aquatic environment of the coastal zone to address questions of algal bloom dynamics, water quality, transient responses to human disturbance, river runoff, and red tides. Phytoplankton functional type (PFT), or biodiversity, can be determined from ocean color using the Phytoplankton Detection with Optics (PHYDOTax) algorithm and this information can be used to detect and monitor for harmful algal blooms. PHYDOTax is sensitive to spectral shape and accurate retrievals of ocean color across the visible spectral range is needed. The specific goal of this paper is to address the challenges of sensor capabilities and atmospheric correction in coastal environments by assessing two atmospheric correction methods using AVIRIS data for the retrieval of ocean color for use in derived products of chlorophyll-*a* and phytoplankton functional type. The atmospheric correction algorithms Atmospheric Removal (ATREM) and Taflkaa were applied to AVIRIS imagery of Monterey Bay, CA collected on 10 April 2013 and 31 October 2013. Data products from the imagery were compared with shipboard measurements including chlorophyll-*a* from whole-water samples and phytoplankton community structure estimated from diagnostic pigment markers using CHEMical TAXonomy (CHEMTAX). Using ATREM and Taflkaa and a selected set of input parameters for the scenes, we were unable to produce accurate retrievals of ocean color for the determination of chlorophyll-*a* and phytoplankton diversity. A modified ATREM correction produced science-quality data in which chlorophyll-*a* was accurately estimated using the Ocean Color 3 (OC3) chlorophyll-*a* algorithm, but biodiversity using PHYDOTax was not accurately estimated. Improvements in sensor calibration, sensitivity, and atmospheric correction of the HypsIRI imagery data set is needed in order to adequately estimate biogeochemically meaningful data products for the ocean such as chlorophyll-*a*, inherent optical properties, or PFTs. The HypsIRI Science Team is seeking improvements so the HypsIRI Airborne Campaign data set can be used for algorithm development to understand biodiversity and ecosystem function of coastal habitats that are facing increasing threats of human impact and climate change.

© 2015 Elsevier Inc. All rights reserved.

1. Introduction

The National Research Council (2007) identified key science questions in its 2007 Decadal Survey to study the world's ecosystems and provide critical information on natural disasters such as wildfires, volcanoes, drought, and harmful algal blooms. The Hyperspectral Infrared Imager (HypsIRI) was borne out of the Decadal Survey and is a proposed satellite sensor for imaging the Earth's surface in the visible to short-

* Corresponding author.

E-mail addresses: sherry.l.palacios@nasa.gov (S.L. Palacios), kudela@ucsc.edu (R.M. Kudela), liane.s.guild@nasa.gov (L.S. Guild), khyashi@ucsc.edu (K.H. Negrey), juan.l.torresperez@nasa.gov (J. Torres-Perez), jbrought@ucsc.edu (J. Broughton).

wave infrared (VSWIR, 380 nm to 2500 nm) at high spectral resolution and in the thermal infrared (TIR, 3–12 μm) as a multispectral sensor (Devred et al., 2013) with a 19-day revisit and ground spatial sampling of 30 m. With respect to aquatic remote sensing, the HypSPIRI mission addresses the following science questions (<http://hypspiri.jpl.nasa.gov/science>):

- 1) How do inland, coastal, and open ocean aquatic ecosystems change due to local and regional thermal climate, land use change, and other factors?
- 2) How do species functional type, and biodiversity composition within ecosystems influence the energy, water, and biogeochemical cycles under varying climatic conditions?
- 3) How is the consumptive use of global freshwater supplies responding to changes in climate and demand, and what are the implications for sustainable management of water resources?
- 4) What is the global spatial pattern of ecosystem and diversity distributions and how do ecosystems differ in their composition or biodiversity?
- 5) What are the seasonal expressions and cycles for terrestrial and aquatic ecosystems, functional groups, and diagnostic species? How are these being altered by changes in climate, land use, and disturbance?
- 6) How are the biogeochemical cycles that sustain life on Earth being altered/disrupted by natural and human-induced environmental change? How do these changes affect the composition and health of ecosystems and what are the feedbacks with other components of the Earth system?
- 7) How do changes in ecosystem composition and function affect human health, resource use, and resource management?

The HypSPIRI Airborne Preparatory Campaign was initiated in 2012 with the objective of collecting representative imaging of terrestrial and aquatic ecosystems over three seasons for three years to capture temporal variability. The mission defined five flight regions in California including coastal areas near Los Angeles, Santa Barbara, Monterey Bay, and San Francisco Bay. Each flight region was imaged in the VIS-SWIR with the Airborne Visible/Infrared Imaging Spectrometer (AVIRIS) sensor and the VIS, NIR, and TIR with the MODIS/ASTER (MASTER) sensor from the high-altitude NASA ER-2 platform to simulate the type of imagery the HypSPIRI sensor would collect. Data sets from the airborne campaign are being used for algorithm development and testing for the future satellite sensor. The primary focus of this study was to

understand how the HypSPIRI sensor might be used to assess water quality and phytoplankton biodiversity in coastal ecosystems. As primary producers, phytoplankton are a vital first step in understanding the fate of oceanic carbon and energy flow. Whether discriminating algae by size, biogeochemical function, or by taxon, high spectral and spatial resolution data are important for developing mathematically sophisticated phytoplankton functional type (PFT) algorithms that can differentiate phytoplankton groups at finer and finer taxonomic scales. The HypSPIRI sensor, with its proposed high spatial and spectral resolution, and inclusion of a thermal sensor will enable more sophisticated PFT and other biological productivity algorithms that depend on coincident ocean color and thermal measurements.

Monterey Bay (Fig. 1) is an open embayment along the central coast of California (USA) that opens to the California Current of the Eastern Pacific. As an eastern boundary current it has thin surface flow that is transported offshore by the combined effect of equator-ward winds and Coriolis-driven mass transport (Ekman Transport). Its circulation has been described extensively elsewhere (Breaker & Broenkow, 1994; Pennington & Chavez, 2000) but follows a climatological trend that includes three seasons characterized by their wind patterns, which in turn affect coastal circulation. Two of the seasons are the focus of this study. From April to August, equator-ward winds are strongest, and coastal upwelling delivers bio-available nutrients to the surface, promoting phytoplankton growth (Smayda & Reynolds, 2001). Diatoms are dominant, including the episodically toxic *Pseudo-nitzschia* (Scholin et al., 2000). During the oceanic season, September to October, equator-ward winds relax, the water column warms and stratifies, and there is a transition to dinoflagellates from diatoms. Many dinoflagellates are susceptible to sheer-stress during upwelling (Smayda, 1997) and have developed strategies to take up nutrients, during periods of resource limitation as found in a warm, stratified water column. Strategies for nutrient uptake include mixotrophy and diel vertical migration to below the thermocline where nutrient concentrations are higher. During the oceanic period, dinoflagellates proliferate to densities that discolor the water and form red tides (Ryan et al., 2009). Red tides in Monterey Bay are rarely toxic, but due to unseasonal reversals in winds that drive upwelling, patchy diatom blooms can occur and mix with the red tides (Fawcett, Pitcher, Bernard, Cembella, & Kudela, 2007). If these diatom blooms are toxic, this can form a second-order harmful algal bloom (HAB) that is also a red tide (Kudela, pers. observation). Recent developments in ocean color algorithms that detect the presence of surface aggregations of phytoplankton (Ryan, Davis,

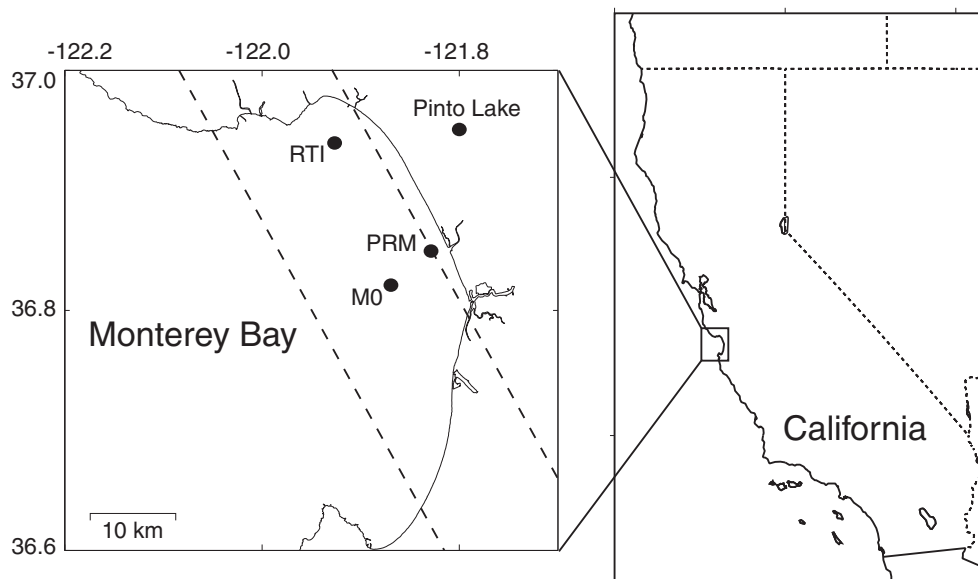


Fig. 1. Study site. Monterey Bay, CA (USA). MO – Legacy M0 Mooring, PRM – Pajaro River Mouth, RTI – Red Tide Incubator, Pinto Lake.

Tufflaro, Kudela, & Gao, 2014) or differentiate between diatoms and dinoflagellates (Palacios, 2012) can improve monitoring efforts of these toxic or nuisance organisms. This capability would enhance the observation potential for warnings of compromised coastal water quality (Frolov, Kudela, & Bellingham, 2013) and would influence decision making for managing coastal ecosystems (e.g., fisheries).

Water quality is a widely-applied and loosely-defined term that generally describes water transparency and its inherent effect on ecosystem health within the water column and the benthos (Kirk, 1994). For the purpose of this study, water quality refers to the optically active constituents within the water column that are used to infer phytoplankton biodiversity. Constituents include phytoplankton, non-algal particles, and chromophoric (or colored) dissolved organic matter (CDOM). Coastal California experiences seasonal variation in phytoplankton biodiversity. Physical and biological forcing drive different phytoplankton taxon-dominated ecosystems and this can have profound effects on ecosystem dynamics and biogeochemical cycling (Ryan et al., 2009; Rykaczewski & Checkley, 2008; Smayda & Reynolds, 2001). The region also has a legacy of harmful algal blooms toxic to both humans and marine animals (Howard, Silver, & Kudela, 2008; Kudela, Lane, & Cochlan, 2008; Kudela, Ryan, Blakely, & Peterson, 2008; Kudela et al., 2005; Ryan et al., 2008; Scholin et al., 2000). Toxic vectoring to commercially harvested fisheries can have disastrous effects on human health, so fisheries are regulated and intensively monitored to prevent illness or loss of human life. These monitoring programs are costly and remote sensing of phytoplankton biodiversity has been explored to improve the efficiency and scope of monitoring efforts (Frolov et al., 2013).

The PFT algorithm, Phytoplankton Detection with Optics (PHYDOTax) was created to differentiate among the major taxa within Monterey Bay to use as a tool for adaptive sampling decisions related to HAB monitoring (Palacios, Peterson, & Kudela, 2012). PHYDOTax is an ocean color algorithm that discriminates phytoplankton taxa contained in a natural sample. It is both a spectral library of representative phytoplankton taxa as well as a linear un-mixing scheme to separate library end-members from the remote sensing reflectance (R_{rs}) spectrum of a natural sample. Among the six phytoplankton taxa differentiated by PHYDOTax (dinoflagellates, diatoms, haptophytes, chlorophytes, cryptophytes, and cyanobacteria), diatoms and dinoflagellates are the groups of most concern in the Monterey Bay as they cause most of the toxic blooms or red tides. PHYDOTax is sensitive to accuracies in spectral shape. Dinoflagellates and diatoms contain some of the same pigments, so their light absorption characteristics are similar, but due to their structure (e.g., cell wall material and shape) their optical backscattering characteristics are different (Dierssen, Kudela, Ryan, & Zimmerman, 2006). The R_{rs} incorporates both of these attributes, and PHYDOTax is able to discriminate between these two groups because of variability in the R_{rs} spectral shape. Any sensor flaws or image pre-processing steps that introduce spurious inflections in the spectrum relative to accurate retrievals from shipboard measurements must be closely evaluated. Atmospheric correction is one such pre-processing step.

Ocean color retrievals in the optically complex waters of the coastal zone can be difficult to achieve due to the presence of optically active constituents in the water column (Carder, Steward, Harvey, & Ortner, 1989), such as high turbidity or CDOM that confound the efficacy of the atmospheric correction algorithms (Gao & Goetz, 1990; Gao, Montes, Ahmad, & Davis, 2000) that rely on the assumption of an optically dark target in the ultraviolet (UV) or near infra-red (NIR). Open ocean waters are typically defined as Case 1, where chlorophyll-a (chl-a) co-varies with other optically active constituents such as CDOM and particle concentration. Case 2 waters are relatively more complex to model as the optically active constituents do not co-vary and each may be controlled by independent physical or biological processes that have little to do with chl-a concentration (Kirk, 1994). Coastal waters are typically Case 2. In these waters, high turbidity or biomass can conflate atmospheric effects, which causes failures in some

algorithms (Ruddick, Ovidio, & Rijkeboer, 2000; Siegel, Wang, Maritorena, & Robinson, 2000). As a result, pixels with otherwise meaningful scientific merit will be flagged and eliminated from study. These failures are a consequence of the legacy of remote sensing efforts in the relatively simpler Case 1 waters where these confounding constituents are less important to the overall water-leaving radiance signal (Gordon, 1997; Gordon & Clark, 1981). When measuring water-leaving radiance, $L_w(\lambda)$, in the blue region of the visible (VIS) domain and in the UV domain, most remote sensing systems exhibit a low signal-to-noise ratio (SNR) and often produce negative values using standard reprocessing methods. These VIS and UV radiances are critical for discriminating pigments from CDOM, potentially useful for identification of features such as red tides, and for use in atmospheric correction. These issues for productive waters include necessitating the use of a nonzero near-infrared (NIR) reflectance in atmospheric correction schemes, which complicates atmospheric correction based on NIR or shortwave infrared (SWIR) wavelengths (Siegel et al., 2000; Werdell, Franz, & Bailey, 2010).

The advent of high spectral resolution (“hyperspectral”) imaging spectrometers further complicates atmospheric correction in Case 2 waters and has led to the development, with continued refinement, of atmospheric correction algorithms that can tolerate higher spectral resolution in these optically complex waters. One algorithm, the Atmospheric Removal Algorithm (ATREM) was developed by Gao, Heidebrecht, and Goetz (1993) for airborne and satellite sensors. Originally developed for terrestrial targets, ATREM was refined for coastal systems. ATREM uses the imagery, radiative transfer modeling of the atmosphere using aerosol and gaseous concentration, and estimates of atmospheric scattering to derive pixel-by-pixel estimates of the atmospheric contribution due to sky-light, and then subtracts that quantity from the at-sensor radiance to obtain surface reflectance. A next generation atmospheric correction algorithm, “The algorithm formerly known as ATREM” (Tafkaa) is a heavily modified version of ATREM. The version used in this study, Tafkaa Tabular (Gao et al., 2000), hereafter referred to as Tafkaa, applies a similar approach but uses a different atmospheric transmittance radiative transfer model than ATREM and also includes a correction for the specular reflection present at the air-sea interface. Error in the spectral shape of ocean color retrievals can vary due to the inputs used for aerosol optical model, aerosol optical depth, column water vapor, relative humidity, or atmospheric gas composition (e.g., ozone, CO, CO₂, N₂O).

An intended outcome of the HypsIRI Airborne Campaign is to develop or refine remote sensing and standard processing algorithms to more rapidly deliver research-ready data to the scientific community to address science questions related to ecosystem function. In order to estimate chl-a or phytoplankton biodiversity from ocean color, it is necessary to accurately remove the atmosphere from retrievals of water-leaving radiance or remote sensing reflectance. The primary objective of this study is to evaluate two atmospheric correction algorithms with respect to estimates of chl-a concentration derived from a standard ocean color algorithm and phytoplankton biodiversity using the spectral shape algorithm, PHYDOTax.

2. Methods

This study was conducted as a part of the HypsIRI Airborne Preparatory Campaign overflights located in California, USA (2013–2015) (<http://hypsiri.jpl.nasa.gov/airborne>). There were five flight “boxes” in the state, one of which was centered over the San Francisco Bay area (Fig. 2) in which Monterey Bay is located. Flight lines were optimized to avoid sun glint on the water surface. Results presented in this study are from two periods in 2013 representing a period of coastal upwelling (10 April 2013) and the oceanic period (31 October 2013). The April collection coincided with a diatom bloom, and the October collection was during a horizontally patchy red tide. High spectral- and spatial-resolution imagery was collected using the Airborne Visible/Infrared



Fig. 2. Flight box for San Francisco Bay. Red lines depict flight vector of NASA ER-2 on 10 April 2013. This flight pattern was repeated for each of three seasons for the HypSIRI Airborne Preparatory Campaign.

Imaging Spectrometer (AVIRIS) and thermal imagery was collected using the MODIS/ASTER Airborne Simulator (MASTER) aboard the NASA ER-2 airborne platform. Only AVIRIS imagery was used in this study.

Concurrent shipboard and land-based measurements of aerosol optical depth (AOD), water-leaving radiance ($L_w(\lambda)$), remote sensing reflectance (R_{rs}), profiles of inherent optical properties (IOPs), size fractionated chl-a concentration, and phytoplankton High Performance Liquid Chromatography (HPLC) pigments were collected for calibration and validation of imagery and algorithms. Imagery data sets were processed through two atmospheric correction schemes, ATREM and Tafkaa. Chl-a concentration and phytoplankton biodiversity were computed using standard chl-a algorithms and PHYDOTax and validated with ground-truth measurements of chl-a and phytoplankton biodiversity.

2.1. Field data

Coincident with overflights, shipboard and land-based calibration and validation measurements were collected to support validation of

the imagery and subsequent data products. Shipboard measurements were collected aboard the *R/V John H. Martin* (Moss Landing Marine Laboratory). There were three ocean stations in Monterey Bay (Fig. 1): the legacy location of the MBARI M0 mooring, the mouth of the Pajaro River (PRM), and the Red Tide Incubator (RTI) (Ryan et al., 2008), and one land-based station at Pinto Lake near the town of Watsonville, CA. While the RTI is a fixed location and often the site of red tides in autumn, the name is a descriptor as red tides can occur in any part of the bay and at times not at the RTI. These represent the “permanent” stations used for calibration and validation of the HypSIRI Airborne data in the Monterey Bay region. They were selected to capture variability in both the R_{rs} and seasonality, including ‘blue’ water, river plume, and high phytoplankton biomass. Relative AOD was measured using a Microtops II Sunphotometer (Solar Light Company) at the Pinto Lake stations, but all other land-based data from this station were used for a corollary study submitted to this special issue (Kudela et al., 2015) and not reported here. Additional land-based measurements that support verification of atmospheric correction approaches included field spectral measurements at an invariant bright target near Moss Landing, CA;

acquired using the Field Spec spectroradiometer (351 nm to 2500 nm; ASD/PANalytics) for use by the AVIRIS data processing team to improve atmospheric correction.

Ship-based water measurements included the underway data acquisition, discrete water samples, and surface and profile measurements of inherent and apparent optical properties (IOPs and AOPs). At each ocean station, we collected discrete samples of surface water to measure size-fractionated chl-a (0.7–1 μm , 1–10 μm , and >10 μm), CDOM, light absorption by phytoplankton and non-algal particles, phytoplankton HPLC-measured pigments, and nutrients. Chl-a was determined following the methods described in Kudela, Cochlan, Peterson, and Trick (2006). Phytoplankton biodiversity was derived using CHEMical TAXonomy, or CHEMTAX (Mackey, Mackey, Higgins, & Wright, 1996), tuned for the California Current System (Anderson, Siegel, Brzezinski, & Guillocheau, 2008). CHEMTAX is a matrix factorization and best fit optimization program for estimating algal class abundances using the ratios of diagnostic algal pigments to chlorophyll-a. CHEMTAX is initiated with a 'best guess' of pigment ratios for a particular region, so a priori knowledge of the algal groups present in a region is needed before implementing this approach to reconstruct algal community composition from HPLC-measured pigments. Diagnostic pigments were used to determine six phytoplankton taxa present in the sample: dinoflagellates, diatoms, haptophytes, chlorophytes, cryptophytes, and cyanobacteria. These in-water phytoplankton biodiversity estimates were used as the in-water validation data set. Measurements of surface and profiling $L_w(\lambda)$ as well as above-water downwelling irradiance were collected using a Satlantic HyperPro II profiling spectroradiometer (350 nm–796 nm). Surface remote sensing reflectance was computed from these measurements with ProSoft 7.7.16 (Satlantic, Inc.) and used in this study to radiometrically estimate chl-a and phytoplankton biodiversity at the sea surface. Profiles and sub-surface measurements of IOPs included optical backscattering at six wavelengths using a HydroScat 6 (420 nm, 442 nm, 470 nm, 510 nm, 590 nm, 700 nm; HOBILabs, Inc.) and total absorption and attenuation at 86 wavelengths using the spectral absorption and attenuation spectrophotometer, AC-S (400 nm to 728 nm; WETLabs, Inc). These IOP measurements are not reported here.

2.2. Airborne image acquisition and atmospheric correction

AVIRIS data were acquired over Monterey Bay on 10 April 2013 and 31 October 2013 from the NASA ER-2 airborne platform flying at an altitude of approximately 20 km. The April 2013 data were from flight number 13-937-00, and include four flight lines that cover Monterey Bay and Pinto Lake. The October 2013 data consist of four flight lines from flight 14-902-00. Over bright targets, such as land, AVIRIS has a peak signal-to-noise ratio of 1000 in the green region (~550 nm) of the visible spectrum, declining to approximately 500 in the near infrared and to below 100 in the UV (Green et al., 1998). The sensor collects data at 224 spectral bands ranging from 380 nm to 2500 nm with a sample interval of 10 nm (Green et al., 1998).

The AVIRIS group at the Jet Propulsion Lab distributed data to the HypSIRI project in several formats. Files used for this study included 1) the L1B non-orthorectored data for use in running the atmospheric correction algorithm Tafkaa by our group, 2) the orthorectored Level 1 B (L1B) data (at-sensor radiance) with associated supporting files (e.g., geo-location files used to orthorectored the Tafkaa-corrected imagery), and 3) the atmospherically corrected and orthorectored L2 data (surface reflectance) distributed by the AVIRIS team. This L2 imagery was corrected using ATREM (http://aviris.jpl.nasa.gov/documents/AVIRIS_HypSIRI_Reflectance_Data.readme) and sampled to a ground sample distance (GSD) of 20 m per pixel. These L2 data were converted to R_{rs} .

ATREM (Gao et al., 1993, 2000) models light absorption and scattering within the atmosphere and from the Earth's surface. It uses as input atmospheric gas concentration, column water vapor, relative humidity,

AOD, aerosol particle size distribution model, viewing geometry, and imager altitude to derive atmospheric transmittance. Scattering in the atmosphere is determined using the Second Simulation of the Satellite Signal in the Solar Spectrum (6S) (Verote, Tanre, Deuze, Herman, & Morcette, 1997). Next, air column water vapor is estimated from the water light-absorption bands at 940 nm and 1140 nm and this is applied to the imagery to obtain surface reflectance (Lambertian surface assumed). Surface reflectance is served to the community by the JPL AVIRIS team as the standard L2 data product.

Tafkaa (Montes & Gao, 2004; Montes, Gao, & Davis, 2001) uses a similar scheme as ATREM, but instead of using 6S, it uses a series of pre-calculated look-up tables for the various atmospheric scattering quantities under different atmospheric scenarios (e.g., maritime, coastal, urban) and also includes the specular effects of the air–sea interface that is lacking in ATREM. Inputs to Tafkaa included the L1B non-orthorectored at-sensor radiance from the AVIRIS sensor, AOD measurements computed from the Microtops II Sunphotometer, ozone from the Ozone Monitoring Instrument (OMI) satellite sensor, and several housekeeping files computed from the image itself, the instrument specifications, and flight heading to compute the R_{rs} pixel-by-pixel for the entire flight line. Data were orthorectored following processing for atmospheric correction, and then spectra from both the ATREM and Tafkaa-corrected imagery were collected at the same location as the ship stations to use for the comparison of imagery and ground-truth observations.

The resultant R_{rs} spectra from both the ATREM and Tafkaa-derived atmospheric correction schemes did not provide realistic results in the blue to green range (400 nm to 520 nm), so we used the ATREM + data provided by the AVIRIS team (processing details below). Reasons for the mismatch may include incorrect input parameters to the atmospheric correction algorithm, problems with the atmospheric correction algorithm itself, low signal-to-noise introducing significant error — a known problem with hyperspectral imagers (Moses, Bowles, Lucke, & Corson, 2012), and the AVIRIS imager not sufficiently calibrated in the blue part of the spectrum for retrievals of the relatively low in-water signal. No one underlying reason could be defined within the scope of this study, so in order to provide science quality data, the JPL AVIRIS team specially corrected one image flightline for each of the two seasons. The correction was performed by empirically fitting the ATREM-corrected image reflectance spectrum co-located with the ground-truth reflectance spectrum collected by the HyperPro spectrometer at a few in situ locations. These forced fits dramatically improved the utility of the image spectra for this study. The new empirically corrected image is hereafter named ATREM+. These ATREM+ data resolved issues with both the atmospheric correction and sensor calibration. The lack of useable data from the ATREM and Tafkaa corrections was due mainly to the input imagery. The underlying theory of the ATREM and Tafkaa algorithms is sound, and it is hoped by the community that these algorithms will continue to evolve as hyperspectral imagers are more widely adopted and knowledge of aerosol optical properties improves. These ATREM and Tafkaa results were retained for the study to highlight problems that may arise as a result of confounding factors such as low sensor signal-to-noise introducing significant error, or to address how atmospheric correction may improve.

Table 1

Error estimate. Remote sensing reflectance. Compared to mean shipboard HyperPro measurements of R_{rs} , ATREM+ had the smallest error (RMSE).

Date	Station	Mean	RMSE		
		HyperPro	ATREM	ATREM +	Tafkaa
10-Apr-13	M0	0.0030	0.0021	0.0006	0.0028
	PRM	0.0059	0.0013	0.0003	0.0030
	RTI	0.0023	0.0020	0.0004	0.0027
31-Oct-13	M0	0.0020	0.0027	0.0006	0.0031
	PRM	0.0014	0.0013	0.0004	0.0015
	RTI	0.0016	0.0017	0.0005	0.0033

A root-mean square error test was used to compare image spectra to ship-based measurements. The ATREM+ method minimized RMSE, compared to the other atmospherically corrected data, and was considered best (Table 1). Regrettably, this method is not scalable to coastal imagery collected for other flightlines on the same day, other flight days, or other flightline locations unless concomitant ground truth data are available or another approach to empirically fit the image spectra can be developed. More work is needed to resolve why the AVIRIS sensor and correction methods are not suitable for ocean color retrievals over a dark target, i.e., optically deep water, without using a case-by-case approach to atmospheric and sensor correction.

2.3. Radiometrically-derived chlorophyll and phytoplankton functional type

Chl-a concentration and phytoplankton biodiversity were derived from radiometric measurements from both the ship-based radiometer and the atmospherically-corrected imagery. The standard OC3 ocean color algorithm (O'Reilly et al., 2000) was used to compute chl-a in the Case 2 waters of Monterey Bay. Chl-a was used as a low threshold validation goal, as the algorithm is widely used and validated, is the ratio of only two spectral bands, and so is less sensitive to subtleties of inflection in the spectral shape that can be the consequence of incorrect atmospheric correction.

Phytoplankton biodiversity was derived with the PFT algorithm, PHYDOTax (Palacios, 2012). PHYDOTax is a semi-analytical linear unmixing algorithm based on first principles of phytoplankton bio-optics. PHYDOTax is composed of a R_{rs} library computed using phytoplankton species-specific inputs of IOPs into the radiative transfer equations (HydroLight™) to derive R_{rs} spectra. Thirteen species common to Monterey Bay were used in the spectral library and included representatives from the diatoms, dinoflagellates, haptophytes, cryptophytes, chlorophytes, and cyanobacteria. The taxon-specific R_{rs} spectra are then normalized to the maximum R_{rs} peak height between 670 nm and 710 nm as a method to normalize by chl-a biomass to produce a quantity, normalized R_{rs} ($R_{rs-norm}$). This approach is similar to normalizing by the Fluorescence Line Height (FLH), an estimate of chlorophyll-a biomass (Abbott & Letelier, 2006). In this approach, the “adaptive peak height” method used allows the peak location to vary, and then normalizes by the true fluorescence peak (Ryan et al., 2014). This allows for a wider range of chlorophyll-a concentrations that may be encountered during a bloom event such as a red tide (Palacios, 2012; Ryan et al., 2014). These spectra were subsetted from 455 nm to 650 nm at 10 nm intervals to form the spectral library. Measured in situ R_{rs} were normalized using the same method and then decomposed into proportions of the representative taxa in the spectral library using an inverse matrix computation. To obtain taxon-specific biomass, these proportions can be multiplied by the chl-a concentration.

2.4. Validation

Validation was performed on the radiometrically-derived chl-a concentration and phytoplankton biodiversity estimates. For chl-a validation, both the ship-based measurements and image-derived chl-a were compared to chl-a measured from water samples using a paired t-test. Both years and stations were pooled for a comparison of six expected chl-a concentrations against six radiometrically determined chl-a concentrations for each of the four treatments: ship-based spectra, spectra from both ATREM corrections, and spectra from the Tafkaa correction. The null hypothesis was no difference between the in-water measured and derived chl-a values, where a critical p-value of 0.05 was used to indicate significance. Validation of phytoplankton biodiversity was performed by comparing CHEMTAX derived phytoplankton taxon proportions to PHYDOTax proportions from the ship-based measurements and those obtained from the imagery using a chi-square cross tabulation. The null hypothesis was no difference between proportions

between the CHEMTAX-derived biodiversity proportions and PHYDOTax-derived proportions from ship-based and image $R_{rs-norm}$ spectra. A critical p-value of 0.05 was used to test significance.

3. Results

3.1. Environmental conditions

Seasonal patterns during both of the overflights were typical of climatology with April being a time of wind-driven coastal upwelling and October a warm stratified oceanic state. The region was experiencing a widespread drought during the sample year and no recent rain events occurred prior to sampling. During April, there was a patchy phytoplankton bloom offshore and within the Monterey Bay. Chlorophyll-a concentrations as high as 60 mg m^{-3} in some regions of the bay were reported from MODIS imagery from the sample day. The phytoplankton assemblage at the Santa Cruz wharf was dominated by diatoms (K. Negrey, pers. obs). The day of the overflight had calm seas and low winds. Aerosol optical depth at 550 nm was 0.095, water vapor was 1.08 cm, and column ozone concentration was 0.258 (these values were used as inputs to the Tafkaa correction). Visibility was clear and there were no clouds over the study area.

In September and October 2013, there was a widespread and horizontally patchy red tide in northern Monterey Bay. The originally scheduled overflight at the beginning of October was postponed due to the government shutdown of 2013, but the red tide persisted beyond its typical climatological window until the end of the month and beyond. This was fortuitous for sampling. On 31 October, a patch of the dinoflagellate-dominated red tide was located at the PRM station with moderate chl-a concentration, 15.90 mg m^{-3} (Table 2). Aerosol optical depth at 550 nm was 0.087, water vapor was 1.3 cm, and column ozone was 0.258. Visibility was clear and there were no clouds over the study area.

3.2. Radiometric observations from ship and imagery

R_{rs} observations were obtained from shipboard measurements and from co-located pixels from the ATREM, ATREM+, and Tafkaa corrected imagery (Fig. 3). The ATREM+ algorithm spectra showed greater fidelity to the ship-based measurements compared to the ATREM and Tafkaa corrections (Table 1). Ship-based HyperPro R_{rs} measurements for April (Fig. 3A–C) show that the PRM had a large peak at 560 nm, consistent with the presence of an algal bloom. Both the RTI and M0 stations had peaks lower than the PRM spectra. Even so, phytoplankton were abundant at all three stations as evidenced by the distinctive peak in the spectra at 560 nm and corresponding trough at 660 nm, and by chl-a concentrations (Fig. 3A–C, Table 2). The April spectra showed a distinctive shoulder between 600 nm and 650 nm, indicative of diatoms (Palacios, 2012). Shipboard observations of R_{rs} in October (Fig. 3D–F) again had distinctive peaks and troughs in all spectra, indicating phytoplankton biomass. Additionally, the M0 station shoaled in the blue part of the spectrum, suggesting the presence of small particles, detritus, or cyanobacteria. In April, the spectral shape and relative magnitudes

Table 2

Chlorophyll-a. Chl-a concentration (mg m^{-3}) from discrete water samples and estimated radiometrically using the OC3 standard chl-a algorithm and R_{rs} spectra at each ocean station and for each correction algorithm evaluated: HyperPro in-water spectra, and the ATREM, ATREM+, and Tafkaa corrections.

Date	Station	Water sample	HyperPro	ATREM	ATREM+	Tafkaa
10-Apr-13	M0	7.43	7.72	1.35	4.64	0.96
	PRM	7.54	5.41	2.99	5.88	1.31
	RTI	9.55	8.08	4.87	6.34	1.13
31-Oct-13	M0	3.06	1.69	0.78	4.38	0.98
	PRM	15.90	10.53	3.7	2.48	3.7
	RTI	11.52	6.68	1.13	2.89	1.11

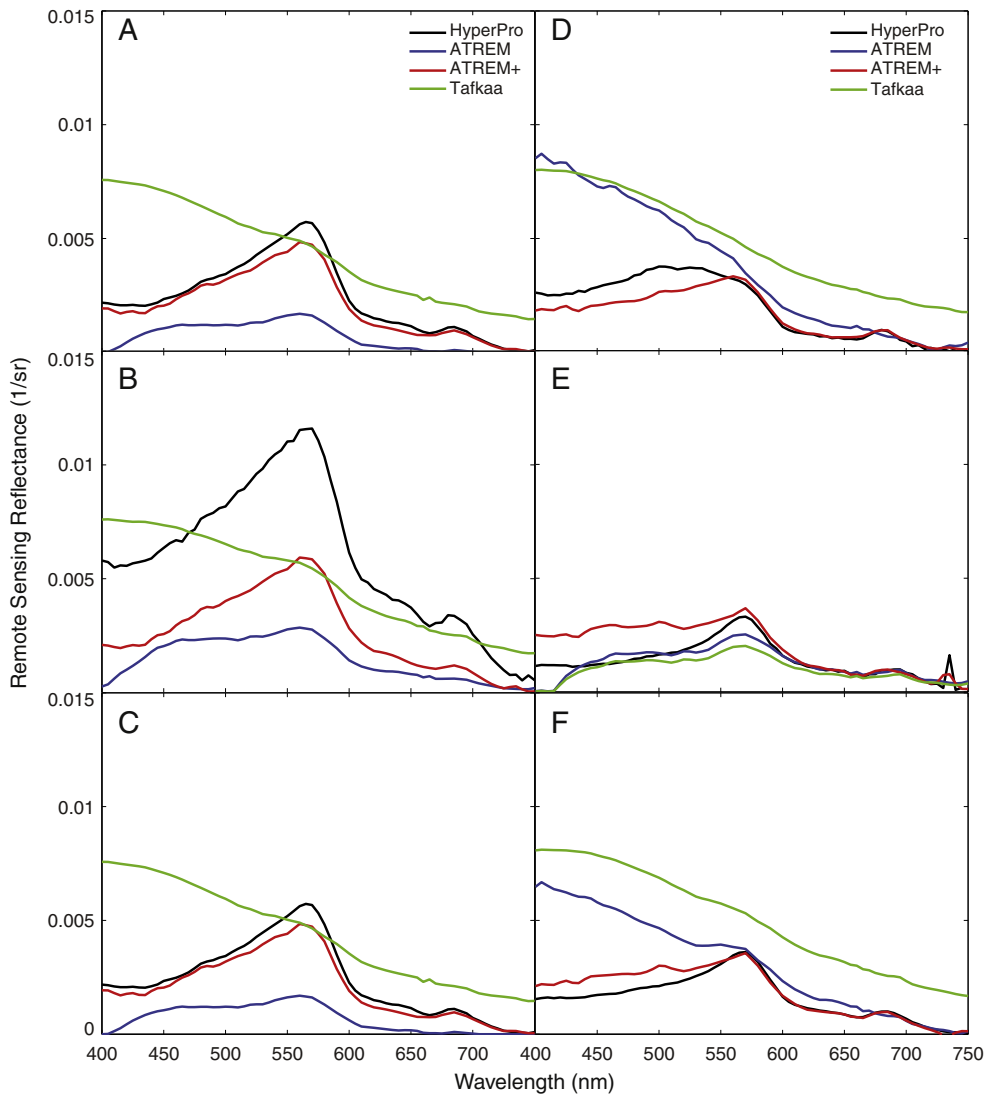


Fig. 3. Remote sensing reflectance spectra for each of the ocean stations. Spectra include ship based HyperPro measurements and spectra from imagery using ATREM, ATREM +, and Tafkaa atmospheric correction. 10 Apr 2013: A) M0, B) PRM, C) RTI. 31 Oct 2013: D) M0, E) PRM, F) RTI.

among stations are preserved in the ATREM + correction from 500 nm to 650 nm, with the exception of Fig. 3B. This is significant as PHYDOTax uses $R_{rs-norm}$ between 455 nm and 650 nm for its library.

3.3. Chlorophyll-a estimates

The chl-a concentrations from whole water samples and estimated from radiometric observations using the standard OC3 chl-a algorithm are presented in Table 2. For all dates and stations, chl-a concentrations (from the water samples) were elevated to bloom levels, or above the 2 to 5 mg m⁻³ background concentration typical of Monterey Bay.

Table 3

Validation of Chl-a. A comparison of measured chlorophyll from water samples and derived chlorophyll from spectra using the OC3 chlorophyll algorithm. A paired t-test was used to evaluate the null hypothesis that the chlorophyll concentrations were the same. In this case, $H_0 = 1$ means that chlorophyll concentrations were different (critical p = 0.05).

Measurement	df	tstat	sd	p-value	H_0
HyperPro	10	1.16	3.72	0.27	0
ATREM	10	3.54	3.28	0.01	1
ATREM +	10	2.16	5.34	0.08	0
Tafkaa	10	4.19	3.16	0.00	1

Radiometric estimates of chl-a using ship-based HyperPro measurements follow a similar pattern in derived chl-a concentration, more so in April than in October when chl-a is underestimated. The ATREM + corrected imagery produced statistically accurate, though weakly correlated in magnitude, chl-a estimates (Table 3, Fig. 4). Chl-a concentration computed from the ATREM and Tafkaa corrected imagery failed to accurately estimate chl-a concentration. Chl-a estimates from radiometry are a low-threshold test as the algorithm uses only two bands. The failure of the standard ATREM and Tafkaa corrections, and the weak fit of ATREM +, suggest that correction of the imagery is in need of improvement.

3.4. Phytoplankton biodiversity

Phytoplankton biodiversity estimated for in-water pigment composition using CHEMTAX and for radiometric estimates using PHYDOTax, are presented in Table 4. Estimates of phytoplankton biodiversity (i.e., dinoflagellates, diatoms, and cyanobacteria) using PHYDOTax is shown for both April and October 2013 in Fig. 5. In-water CHEMTAX estimates in April suggest a diatom dominated system at all three stations at 52–67% of the population, with cyanophytes composing 18–24% of the community. Cryptophytes are estimated to be present only at the PRM and M0 stations at 13% and 20%, respectively. These in-water

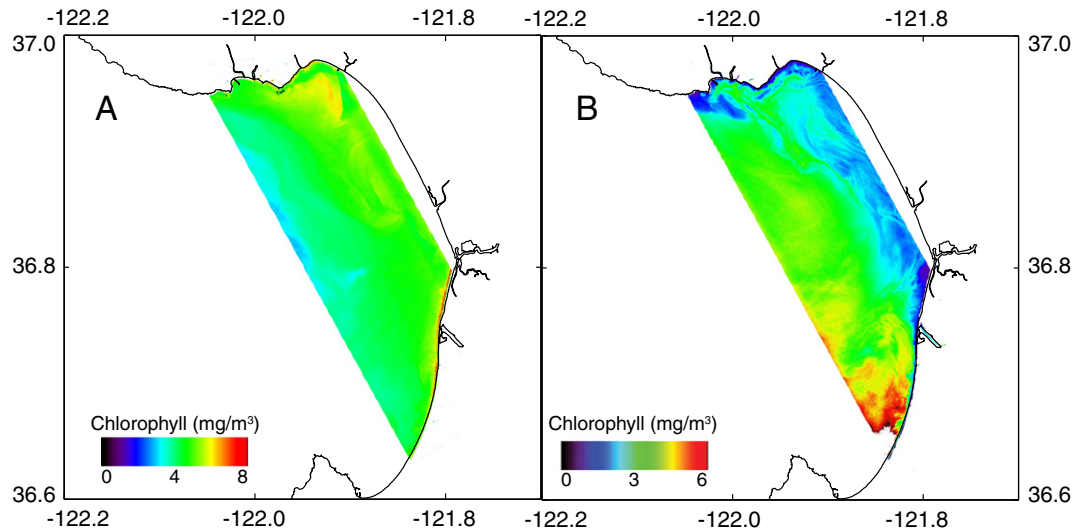


Fig. 4. Chlorophyll-a. Chlorophyll-a concentration derived from the OC3 ocean color algorithm applied to the ATREM + atmospheric corrected imagery. A) 10 Apr 2013, B) 31 Oct 2013.

CHEMTAX population estimates were compared to the ship-based HyperPro radiometric measurements as a test of how well PHYDOTax was working. The patterns of relative abundance of each taxon were not statistically significant for most of the stations on either of the dates (Table 5). Nevertheless, trends in taxon composition did exist during the 10 April 2013 collection (Table 4). The ATREM + -based

Table 4

Phytoplankton functional types. Proportions of each phytoplankton taxon, determined from CHEMTAX using in-water diagnostic HPLC pigments, and from PHYDOTax using normalized R_{rs} measurements from shipboard HyperPro observations, ATREM, ATREM +, and Tafkaa corrected imagery spectra. Dino = dinoflagellate, hapto = haptophyte, chloro = chlorophyte, crypto = cryptophyte, cyano = cyanophyte.

10-Apr-13							
Station	Input	Dino	Diatom	Hapto	Chloro	Crypto	Cyano
MO	In-water	0.01	0.55	0.04	0.01	0.20	0.18
MO	HyperPro	0.12	0.67	0.00	0.00	0.00	0.21
MO	ATREM	0.36	0.44	0.05	0.16	0.00	0.00
MO	ATREM +	0.18	0.58	0.02	0.00	0.00	0.22
MO	Tafkaa	0.39	0.40	0.08	0.09	0.03	0.00
PRM	In-water	0.03	0.52	0.06	0.02	0.13	0.24
PRM	HyperPro	0.13	0.71	0.02	0.00	0.00	0.13
PRM	ATREM	0.27	0.62	0.04	0.00	0.00	0.07
PRM	ATREM +	0.18	0.58	0.02	0.00	0.00	0.22
PRM	Tafkaa	0.40	0.38	0.08	0.08	0.05	0.00
RTI	In-water	0.09	0.67	0.01	0.02	0.00	0.21
RTI	HyperPro	0.07	0.64	0.05	0.00	0.00	0.25
RTI	ATREM	0.23	0.68	0.01	0.05	0.00	0.04
RTI	ATREM +	0.21	0.58	0.03	0.00	0.00	0.19
RTI	Tafkaa	0.40	0.38	0.09	0.10	0.04	0.00
31-Oct-13							
Station	Input	Dino	Diatom	Hapto	Chloro	Crypto	Cyano
MO	In-water	0.42	0.12	0.30	0.03	0.10	0.02
MO	HyperPro	0.31	0.36	0.01	0.00	0.22	0.10
MO	ATREM	0.34	0.50	0.06	0.08	0.02	0.00
MO	ATREM +	0.39	0.47	0.00	0.02	0.05	0.06
MO	Tafkaa	0.40	0.38	0.08	0.08	0.06	0.00
PRM	In-water	0.89	0.03	0.03	0.01	0.03	0.01
PRM	HyperPro	0.59	0.31	0.01	0.08	0.01	0.00
PRM	ATREM	0.29	0.69	0.02	0.00	0.00	0.00
PRM	ATREM +	0.44	0.43	0.00	0.05	0.01	0.06
PRM	Tafkaa	0.29	0.69	0.02	0.00	0.00	0.00
RTI	In-water	0.92	0.00	0.02	0.01	0.04	0.00
RTI	HyperPro	0.57	0.34	0.02	0.00	0.07	0.00
RTI	ATREM	0.36	0.45	0.07	0.11	0.00	0.00
RTI	ATREM +	0.49	0.40	0.01	0.10	0.00	0.00
RTI	Tafkaa	0.40	0.39	0.08	0.07	0.05	0.00

estimates were consistent with the predictions from the HyperPro measurements, but the ATREM and Tafkaa-based estimates were not for April. PHYDOTax failed to accurately predict biodiversity for 31 October 2013, except for the PRM (Table 5). The predicted community structure was statistically different from the in-water estimates and the proportions did not appear to follow any clear trend on this date as they did in April 2013. This was a period of an intense and patchy dinoflagellate bloom, especially so at the PRM and RTI stations as evidenced in the in-water estimates. PHYDOTax mostly failed to adequately discriminate between diatoms and dinoflagellates for October (Table 5) for the ship-based radiometric spectra and the image spectra. The dominant dinoflagellate genus was *Ceratium*, a large, armored peridinin-containing dinoflagellate. This mismatch suggests that more work is needed to refine PHYDOTax in its skill differentiating between diatoms and dinoflagellates.

4. Discussion

The modified ATREM correction, ATREM +, produced an adequate HypsIRI simulation data product for remote sensing reflectance for use in developing and refining water quality and phytoplankton biodiversity algorithms in the coastal zone. The OC3 chl-a algorithm accurately estimated surface chl-a concentrations for the ship-based radiometry spectra and weakly for the ATREM + spectra for both April and October 2013. The PHYDOTax-derived biodiversity estimates from ship-based radiometry measurements were not statistically significant but did follow the same demographic trends in April as the ground-truth data set derived from CHEMTAX. This was not the case for October 2013. The lack of a trend and statistical significance of the ship-based PHYDOTax estimates warrants further study and refinement of the PHYDOTax algorithm. A more direct cell-enumeration instrument like the Imaging Flow Cytobot (Olson & Sosik, 2007; Sosik & Olson, 2007), not available for this study, would have provided a more credible validation data set for PHYDOTax than the error-prone CHEMTAX approach. When comparing PHYDOTax biodiversity estimates derived from image retrievals to the ship-based radiometric estimates, ATREM + had the best fit for both April and October.

The proposed HypsIRI satellite is expected to deliver information and data products for a wide range of habitats to understand the world's ecosystems and provide critical information on natural disasters such as wildfires, volcanoes, drought, and harmful algal blooms. To meet this ambitious goal, the proposed sensor suite will collect information from the ultraviolet to the visible, near infrared, short-wave infrared, and into the thermal spectral range at hyperspectral (UV-SWIR) and

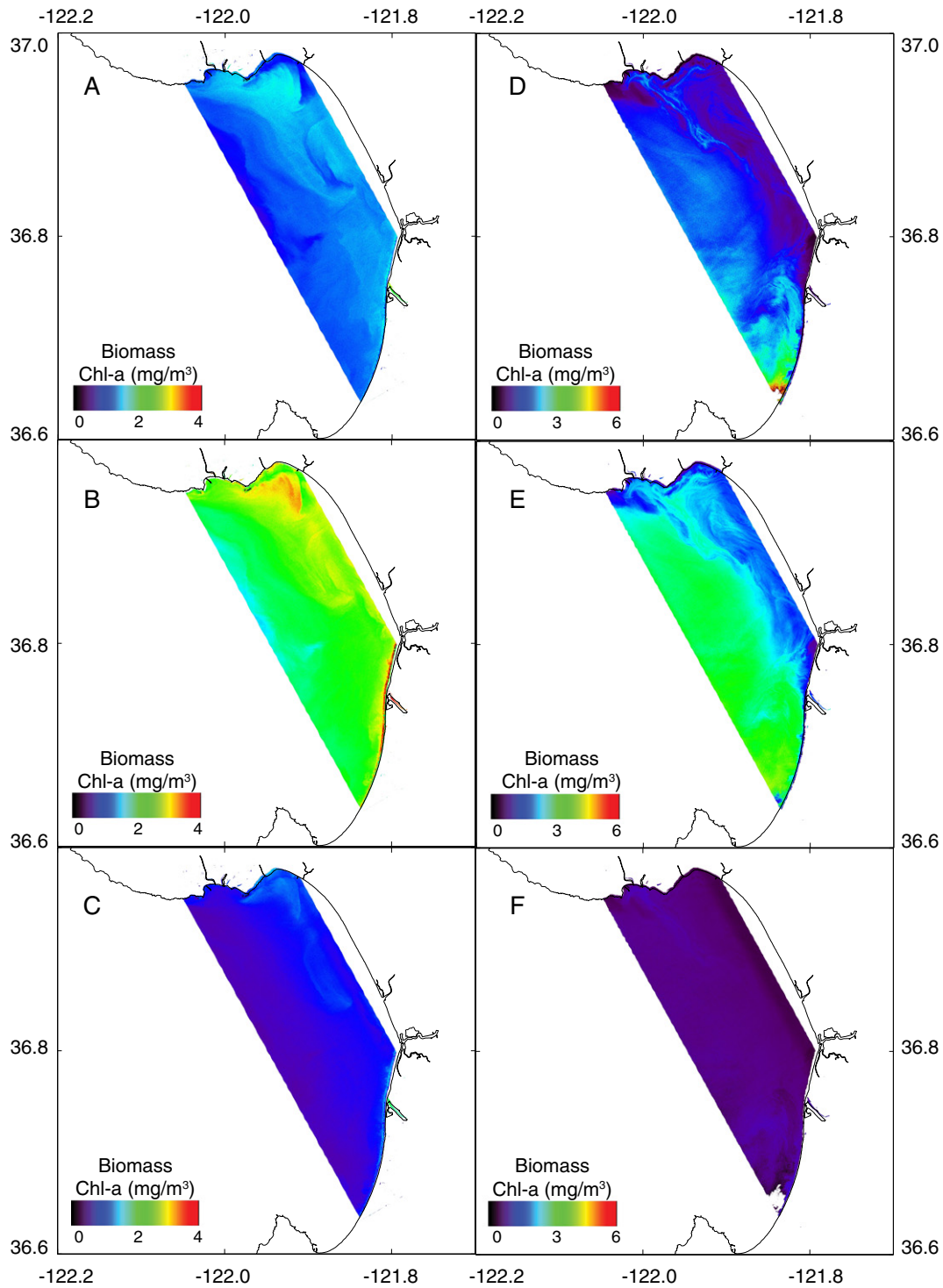


Fig. 5. Phytoplankton biodiversity – PHYDOTax estimates. Taxon-specific biomass estimated for dinoflagellates, diatoms, and cyanobacteria using PHYDOTax applied to the ATREM + atmospheric corrected imagery. 10 Apr 2013: A) dinoflagellates, B) diatoms, C) cyanobacteria. 31 Oct 2013: D) dinoflagellates, E) diatoms, F) cyanobacteria.

multispectral (TIR) resolution, at a spatial scale of 60 m GSD, with a 19-day return rate. Competing interests necessarily influence the development of this satellite sensor suite to optimally image the Earth to address the science questions put forth by the Decadal Survey.

The Case 2 waters of the coastal zone have special needs with respect to sensor sensitivity, sensor calibration (Kohler, Bissett, Steward, & Davis, 2004), dark pixel constraints (Gao & Davis, 1997), and atmospheric correction (Gao & Goetz, 1990). The ocean is a radiometrically dark target with a surface albedo in the range of 5–10% (Kirk, 1994).

As a result, image sensors collecting light emitted from optically deep ocean targets must have the appropriate sensitivity, or SNR, for such an environment. Historically, imager SNR is optimized in the green (~550 nm) part of the visible spectrum with decreasing SNR towards the blue and UV and also towards the NIR (Moses et al., 2012), as is the case with the AVIRIS sensor (Green et al., 1998). Sensor design for dark ocean targets must reconcile the competing need for high SNR throughout the visible range and high dynamic range (or saturation radiance) in the NIR in order to both quantify small magnitude differences

Table 5

Validation of phytoplankton functional types. A comparison between expected proportions (computed from ship-based $R_{rs-norm}$ spectra) and observed from two atmospheric correction algorithms applied to imagery. H0 – no difference between proportions, reject H0 if χ^2 is greater than expected χ^2 (df = 6, expected $\chi^2 = 12.8$).

Station	Measurement	10-Apr-13			31-Oct-13		
		χ^2	p-Value	Reject H0	χ^2	p-Value	Reject H0
M0	HyperPro	14.0	0.30	Y	30	0.22	Y
M0	ATREM	18.0	0.32	Y	30	0.22	Y
M0	ATREM +	19.5	0.24	Y	30	0.22	Y
M0	Tafkaa	24.0	0.24	Y	24.0	0.24	Y
PRM	HyperPro	18.0	0.26	Y	12.0	0.15	N
PRM	ATREM	24.0	0.24	Y	8.6	0.19	N
PRM	ATREM +	24.0	0.24	Y	12.0	0.29	N
PRM	Tafkaa	24.0	0.24	Y	8.6	0.19	N
RTI	HyperPro	24.0	0.24	Y	19.5	0.24	Y
RTI	ATREM	30.0	0.22	Y	19.5	0.24	Y
RTI	ATREM +	24.0	0.24	Y	19.5	0.24	Y
RTI	Tafkaa	30.0	0.22	Y	24.0	0.24	Y

in ocean properties and to permit the range needed for atmospheric correction using NIR bands (Hu et al., 2012). Hu et al. (2012) proposed the following SNR for the future GEO-CAPE mission: >1000 for λ between 350 and 720, >600 for 720–900 nm, and >100–200 for the shortwave infrared (SWIR). Aquatic constituents, chl-a, detritus, CDOM, and water itself, are optically active in the blue to green region of the spectrum. A sensor with fair to poor SNR in those regions of the spectrum will perform poorly in capturing the signal needed to accurately characterize the true ocean color and will result in inaccurate derived products. This problem is especially acute for coastal remote sensing in Case 2 waters where sediment plumes, re-suspended sediment, and runoff of terrestrially-derived CDOM may be present and absorbing light in the blue part of the spectrum. The SNR for hyperspectral sensors should be optimized in the blue to green range of the spectrum in order to accurately retrieve ocean color (Moses et al., 2012). Additionally, sensor calibration must include the full visible spectrum, and not be red-biased which is typically the case using integrating sphere calibration methods alone (Kohler et al., 2004). The AVIRIS sensor used for the HypSIIRI Airborne Campaign lacked the appropriate SNR and calibration in the blue to green range (Green et al., 1998). Estimates of ocean chl-a would be improved with higher sensitivity and better calibration in the blue to green region of the visible spectrum. A promising new sensor, the Portable Remote Imaging Spectrometer (PRISM) is a push-broom sensor that captures imagery in the 350 nm–1050 nm range, with a separate spot radiometer at 1240 nm and 1610 nm for use in atmospheric correction. PRISM offers higher SNR and spectral resolution in the 380 nm–600 nm range (Mouroulis et al., 2014) and provides adequate SNR for ocean applications. Use of this sensor in future HypSIIRI Airborne Campaigns would overcome many of the shortcomings of the AVIRIS sensor over water and provide a demonstration data set appropriate for ocean color algorithm development and refinement. The PRISM sensor may provide a model for the development of the future HypSIIRI UV-SWIR sensor.

Atmospheric correction poses a major challenge in the Case 2 waters of the coastal zone. Atmospheric correction takes into account the surface reflectance, the absorption of light by atmospheric gases, and the scattering and absorption of light by atmospheric aerosols. These processes are incorporated into an atmospheric radiative transfer model to determine the radiance attributed to atmospheric constituents and geometry so that it can be subtracted from the at-sensor radiance measured by the imaging spectrometer. Inputs to the atmospheric correction algorithm include sensor geometry, a pre-defined aerosol model, column water vapor, relative humidity, ozone and other atmospheric gases, aerosol optical depth at 550 nm (typically), and surface geometry (Gao & Davis, 1997; Gao et al., 2000; Montes et al., 2001). Aerosols are responsible for approximately 80% of scattered light in the atmosphere

(Mobley, Boss, Roesler, & Taylor, 2015). All aerosols scatter light and some aerosols absorb strongly in the blue to green region of the spectrum. Poorly constrained inputs into the correction algorithm will result in inaccurate ocean color retrievals. ATREM, and other atmospheric correction algorithms, use five pre-defined aerosol models (coastal, coastal-a, maritime, urban, and tropospheric), which characterize the uni- or bi-modal distribution of aerosol particle size distribution in the atmosphere. Recently, Ahmad et al. (2010), proposed an expansion of the number of possible aerosol models to account for more realistic aerosol particle size distributions found in nature. This is especially relevant for the coastal ocean where a mixture of aerosol model type may be present (e.g., both urban and coastal).

A re-evaluation of atmospheric correction, especially for the coastal zone, is needed. The surface retrievals from the proposed HypSIIRI sensor would greatly benefit from such an effort to build innovative new methods for atmospheric correction in the coastal zone. These methods include the addition of concomitant surface imaging spectrometry and atmospheric measurements. Ground-based Aerosol Robotic Network (AERONET) and AERONET with Ocean Color measurements (AERONET-OC) stations provide this information (Zibordi et al., 2006). AERONET-OC stations are sparsely distributed, so an important pathway to improved atmospheric correction is coincident imagery and atmospheric measurements from airborne platforms. Atmospheric measurements can be used to inform the atmospheric correction algorithm and improve ocean color retrievals. In addition to innovative methods to collect calibration and validation data sets, the correction algorithms themselves need improvement. Areas of consideration include: 1) increasing the number and diversity of aerosol models, 2) enable the use of AOD at more than just 550 nm, 3) include the capability to incorporate horizontal heterogeneity of aerosols into the correction algorithm to account for dynamic atmospheric conditions at the land–sea interface, 4) allow for increased flexibility in computing vertical structure of the atmospheric column, 5) address problems with thresholds that flag and remove bright pixels (e.g., river plumes and algal blooms), and 6) re-consider the dark pixel assumption at 865 nm in coastal waters. The sensor community has acknowledged some of the issues related to SNR, calibration, and atmospheric correction and is working to address those problems (e.g., by sampling in the SWIR for dark pixels Mouroulis et al., 2014).

There is great anticipation in the aquatic sciences community for the proposed HypSIIRI sensor (Devred et al., 2013). The Hyperspectral Imager for the Coastal Ocean (HICO) was an experimental sensor on the International Space Station from September 2009 to September 2014. It was a targeted sensor that provided hyperspectral ocean color retrievals (400 nm–900 nm) at 90 m GSD. It was operational for four years beyond its expected lifetime and has provided a valuable demonstration data set for the coastal and inland aquatic remote sensing community. Between the HypSIIRI Aquatic Sciences Group (renamed Aqua RS) and the more international HICO User's Group, a number of innovative studies have been reported. The existing body of work using HICO includes seagrass mapping (Cho et al., 2014), bathymetry mapping (Z. Lee pers. comm.), water quality (Braga et al., 2013; Kudela et al., 2015), red tide detection (Ryan et al., 2014), improved chl-a detection (Moses et al., 2013), cloud removal (Gao & Li, 2012), harmful cyanobacteria bloom detection (Kudela et al., 2015), and internal wave detection. The hyperspectral data sets delivered by HICO and proposed by HypSIIRI will enable the development of more sophisticated ocean color algorithms that exploit the data richness of the high resolution data. With the high spectral and spatial resolution data sets, and with the loss of HICO, these types of studies are possible only with the proposed HypSIIRI sensor. At 1 km per pixel resolution, the proposed PACE satellite sensor lacks the spatial resolution needed for the finer scale dynamics in the coastal zone or inland waters. Loss of HICO in 2014 opened a void for coastal imaging that will not be filled by PACE. In the current NASA satellite mission plan, only the HypSIIRI sensor will fill this important gap at the land–sea interface and for inland waters.

Accurate ocean color retrievals are imperative to assessing ecosystem status in the coastal zone. Improvements in sensor sensitivity, sensor calibration, and atmospheric correction are likely the best opportunity to constrain errors in retrievals. Until accurate ocean retrievals are possible, the promise of a high resolution imaging spectrometer for the coastal zone, such as HypSPIRI, will fall short of the goal to study the world's ecosystems and to provide critical information on ecosystem function and natural disasters such as harmful algal blooms.

Acknowledgments

Funding to support this research was provided by NASA's Research Opportunities in Space and Earth Science (ROSES-2011), NNN11ZDA001N, Program Element A.26: HypSPIRI Preparatory Airborne Activities and Associated Science and Applications Research. Funding was provided to SP from the NASA Postdoctoral Program Fellowship (RO 18729) administered by the Oak Ridge Affiliated Universities (ORAU). SP wishes to thank B.C. Gao, R.O. Green, D.R. Thompson, M. Peacock, I. McCubbin, and R. Pasetto for technical assistance. We thank the editors of the HypSPIRI special issue for making this opportunity possible. We are very grateful to the two anonymous reviewers who helped improve the manuscript with thoughtful suggestions and guidance.

References

- Abbott, M.R., & Letelier, R.M. (2006). *Algorithm theoretical basis document: Chlorophyll fluorescence (MODIS product number 20)*. In .
- Ahmad, Z., Franz, B.A., McClain, C.R., Kwiatkowska, E.J., Werdell, P.J., Shettle, E.P., et al. (2010). New aerosol models for the retrieval of aerosol optical thickness and normalized water-leaving radiances from the SeaWiFS and MODIS sensors over coastal regions and open oceans. *Applied Optics*, 49, 5545–5560.
- Anderson, C.R., Siegel, D.A., Brzezinski, M.A., & Guillocheau, N. (2008). Controls on temporal patterns in phytoplankton community structure in the Santa Barbara Channel, California. *Journal of Geophysical Research*, 113.
- Braga, F., Giardino, C., Bassani, C., Matta, E., Candiani, G., Strombeck, N., et al. (2013). Assessing water quality in the northern Adriatic Sea from HICO data. *Remote Sensing Letters*, 4, 1028–1037.
- Breaker, L.C., & Broenkow, W.W. (1994). The circulation of Monterey Bay and related processes. *Oceanography and Marine Biology*, 32, 1–64.
- Carder, K.L., Steward, R.G., Harvey, G.R., & Ortner, P.B. (1989). Marine humic and fulvic acids – Their effects on remote-sensing of ocean chlorophyll. *Limnology and Oceanography*, 34, 68–81.
- Cho, H.J., Ogashawara, I., Mishra, D., White, J., Kameron, A., Morris, L., et al. (2014). Evaluating Hyperspectral Imager for the Coastal Ocean (HICO) data for seagrass mapping in Indian River Lagoon, FL. *GIScience & Remote Sensing*, 51, 120–138.
- Devred, E., Turpie, K.R., Moses, W., Klemas, V.V., Moisan, T.A.H., Babin, M., et al. (2013). Future retrievals of water column bio-optical properties using the Hyperspectral Infrared Imager (HypSPIRI). *Remote Sensing*, 5, 6812–6837.
- Dierssen, H.M., Kudela, R.M., Ryan, J.P., & Zimmerman, R.C. (2006). Red and black tides: Quantitative analysis of water-leaving radiance and perceived color for phytoplankton, colored dissolved organic matter, and suspended sediments. *Limnology and Oceanography*, 51, 2646–2659.
- Fawcett, A., Pitcher, G.C., Bernard, S., Cembella, A.D., & Kudela, R.M. (2007). Contrasting wind patterns and toxigenic phytoplankton in the southern Benguela upwelling system. *Marine Ecology—Progress Series*, 348, 19–31.
- Frolov, S., Kudela, R.M., & Bellingham, J.G. (2013). Monitoring of harmful algal blooms in the era of diminishing resources: A case study of the US West Coast. *Harmful Algae*, 21–22, 1–12.
- Gao, B.C., & Davis, C. (1997). Development of a line-by-line-based atmosphere removal algorithm for airborne and spaceborne imaging spectrometers. *SPIE*, 3118, 132–141.
- Gao, B.C., & Goetz, A.F.H. (1990). Column atmospheric water vapor and vegetation liquid water retrievals from Airborne Imaging Spectrometer data. *Journal of Geophysical Research*, 95, 3549–3564.
- Gao, B.C., Heidebrecht, K.B., & Goetz, A.F.H. (1993). Derivation of scaled surface reflectances from AVIRIS data. *Remote Sensing of Environment*, 44, 165–178.
- Gao, B.C., & Li, R.R. (2012). Removal of thin cirrus scattering effects for remote sensing of ocean color from space. *IEEE Geoscience and Remote Sensing Letters*, 9, 972–976.
- Gao, B.C., Montes, M.J., Ahmad, Z., & Davis, C.O. (2000). Atmospheric correction algorithm for hyperspectral remote sensing of ocean color from space. *Applied Optics*, 39, 887–896.
- Gordon, H.R. (1997). Atmospheric correction of ocean color imagery in the Earth Observing System era. *Journal of Geophysical Research—Atmospheres*, 102, 17081–17106.
- Gordon, H.R., & Clark, D.A. (1981). Clear water radiances for atmospheric correction of coastal zone color scanner imagery. *Applied Optics*, 20, 4175–4180.
- Green, R.O., Eastwood, M.L., Sarture, C.M., Chrien, T.G., Aronsson, M., Chippendale, B.J., et al. (1998). Imaging spectroscopy and the Airborne Visible/Infrared Imaging Spectrometer (AVIRIS). *Remote Sensing of Environment*, 65, 227–248.
- Howard, M., Silver, M., & Kudela, R.M. (2008). Yessotoxin detected in mussel (*Mytilus californicus*) and phytoplankton samples from the US west coast. *Harmful Algae*, 7, 646–652.
- Hu, C.M., Feng, L., Lee, Z., Davis, C.O., Mannino, A., McClain, C.R., et al. (2012). Dynamic range and sensitivity requirements of satellite ocean color sensors: Learning from the past. *Applied Optics*, 51, 6045–6062.
- Kirk, J.T.O. (1994). *Light and photosynthesis in aquatic ecosystems*. New York: Cambridge University Press.
- Kohler, D., Bissett, W.P., Steward, R.G., & Davis, C. (2004). New approach for the radiometric calibration of spectral imaging systems. *Optics Express*, 12, 2463–2477.
- Kudela, R.M., Cochlan, W.P., Peterson, T.D., & Trick, C.G. (2006). Impacts on phytoplankton biomass and productivity in the Pacific Northwest during the warm ocean conditions of 2005. *Geophysical Research Letters*, 33, L22506 <http://dx.doi.org/10.1029/2006GL026772>.
- Kudela, R.M., Lane, J.Q., & Cochlan, W.P. (2008). The potential role of anthropogenically derived nitrogen in the growth of harmful algae in California, USA. *Harmful Algae*, 8, 103–110.
- Kudela, R.M., Palacios, S.L., Austerberry, D.C., Accorsi, E.K., Guild, L.S., & Torres-Perez, J.L. (2015). Application of hyperspectral remote sensing to cyanobacterial blooms in inland waters. *Remote Sensing of Environment, HypSPIRI Special Issue* (<http://www.sciencedirect.com/science/article/pii/S0034425715000437#>).
- Kudela, R.M., Pitcher, G.C., Probyn, T.A., Figueiras, F., Moita, M., & Trainer, V. (2005). Harmful algal blooms in coastal upwelling systems. *Oceanography*, 18, 184–197.
- Kudela, R.M., Ryan, J., Blakely, M.D., & Peterson, T.D. (2008). Linking the physiology and ecology of *Cochlodinium* to better understand harmful algal bloom events: A comparative approach. *Harmful Algae*, 7, 278–292.
- Mackey, M.D., Mackey, D.J., Higgins, H.W., & Wright, S.W. (1996). CHEMTAX – A program for estimating class abundances from chemical markers: Application to HPLC measurements of phytoplankton. *Marine Ecology—Progress Series*, 144, 265–283.
- Mobley, C.D., Boss, E., Roesler, C., & Taylor, L. (2015). *Ocean optics web book In*.
- Montes, M.J., & Gao, B.C. (2004). *NRL atmospheric correction algorithms for oceans: Tafkaa user's guide*. In Naval Research Laboratory, 1–39.
- Montes, M.J., Gao, B.C., & Davis, C.O. (2001). A new algorithm for atmospheric correction of hyperspectral remote sensing data. *SPIE*, 4382, 23–30.
- Moses, W.J., Bowles, J.H., Lucke, R.L., & Corson, M.R. (2012). Impact of signal-to-noise ratio in a hyperspectral sensor on the accuracy of biophysical parameter estimation in case II waters. *Optics Express*, 20, 4309–4330.
- Moses, W.J., Gitelson, A.A., Berdnikov, S., Bowles, J.H., Povazhnyi, V., Sapryngin, V., et al. (2013). HICO-based NIR-red models for estimating chlorophyll-a concentration in productive coastal waters. *IEEE Geoscience and Remote Sensing Letters*, 11, 1111–1115.
- Mouroulis, P., Van Gorp, B., Green, R.O., Dierssen, H.M., Wilson, D.W., Eastwood, M.L., et al. (2014). Portable Remote Imaging Spectrometer coastal ocean sensor: Design, characteristics, and first flight results. *Applied Optics*, 53, 1363–1380.
- National Research Council (2007). *Earth science and applications from space: National imperatives for the next decade and beyond*. Washington, DC: The National Academies Press 0-309-66714-3, 456.
- Olson, R.J., & Sosik, H.M. (2007). A submersible imaging-in-flow instrument to analyze nano- and microplankton: Imaging FlowCytobot. *Limnology and Oceanography: Methods*, 5, 195–203.
- O'Reilly, J.E., Maritorena, S., O'Brien, M.C., Siegel, D.A., Toole, D., Menzies, D., et al. (2000). SeaWiFS postlaunch calibration and validation analyses, part 3. In S.B. Hooker, & E.R. Firestone (Eds.), *NASA tech. memo. 2000-206892* (pp. 49). NASA Goddard Space Flight Center.
- Palacios, S.L. (2012). Identifying and tracking evolving water masses in optically complex aquatic environments. *Ocean Sciences*. Santa Cruz: University of California—Santa Cruz.
- Palacios, S.L., Peterson, T.D., & Kudela, R.M. (2012). Optical characterization of water masses within the Columbia River Plume. *Journal of Geophysical Research—Oceans*, 117.
- Pennington, J.T., & Chavez, F.P. (2000). Seasonal fluctuations of temperature, salinity, nitrate, chlorophyll and primary production at station H3/M1 over 1989–1996 in Monterey Bay, California. *Deep-Sea Research Part II*, 47, 947–973.
- Ruddick, K.G., Ovidio, F., & Rijkeboer, M. (2000). Atmospheric correction of SeaWiFS imagery for turbid coastal and inland waters. *Applied Optics*, 39, 897–912.
- Ryan, J.P., Davis, C.O., Tufflaro, N.B., Kudela, R.M., & Gao, B.C. (2014). Application of the hyperspectral imager for the coastal ocean to phytoplankton ecology studies in Monterey Bay, CA USA. *Remote Sensing*, 6, 1007–1025.
- Ryan, J.P., Fischer, A.M., Kudela, R.M., Gower, J.F.R., King, S.A., Marin, R., et al. (2009). Influences of upwelling and downwelling winds on red tide bloom dynamics in Monterey Bay, California. *Continental Shelf Research*, 29, 785–795.
- Ryan, J.P., Gower, J.F.R., King, S.A., Bissett, W.P., Fischer, A.M., Kudela, R.M., et al. (2008). A coastal ocean extreme bloom incubator. *Geophysical Research Letters*, 35.
- Ryckaczewski, R.R., & Checkley, D.M. (2008). Influence of ocean winds on the pelagic ecosystem in upwelling regions. *Proceedings of the National Academy of Sciences of the United States of America*, 105, 1965–1970.
- Scholin, C.A., Gulland, F., Doucette, G.J., Benson, S., Busman, M., Chavez, F.P., et al. (2000). Mortality of sea lions along the central California coast linked to a toxic diatom bloom. *Nature*, 403, 80–84.
- Siegel, D.A., Wang, M., Maritorena, S., & Robinson, W.D. (2000). Atmospheric correction of satellite ocean color imagery: The black pixel assumption. *Applied Optics*, 39, 3582–3591.
- Smayda, T.J. (1997). Harmful algal blooms: Their ecophysiology and general relevance to phytoplankton blooms in the sea. *Limnology and Oceanography*, 42, 1137–1153.
- Smayda, T.J., & Reynolds, C.S. (2001). Community assembly in marine phytoplankton: Application of recent models to harmful dinoflagellate blooms. *Journal of Plankton Research*, 23, 447–461.

- Sosik, H.M., & Olson, R.J. (2007). Automated taxonomic classification of phytoplankton sampled with imaging-in-flow cytometry. *Limnology and Oceanography: Methods*, 5, 204–216.
- Vermote, E.F., Tanre, D., Deuze, J.L., Herman, M., & Morcette, J.J. (1997). Second simulation of the satellite signal in the solar spectrum, 6S: An overview. *IEEE Geoscience and Remote Sensing Letters*, 35, 675–686.
- Werdell, P.J., Franz, B.A., & Bailey, S.W. (2010). Evaluation of shortwave infrared atmospheric correction for ocean color remote sensing of Chesapeake Bay. *Remote Sensing of Environment*, 114, 2238–2247.
- Zibordi, G., Holben, B.N., Hooker, S.B., Melin, F., Berthon, J.F., Slutsker, I., et al. (2006). A network for standardized ocean color validation measurements. *EOS Transactions*, 87, 293–304.